NEAR THRESHOLD FATIGUE CRACK PROPAGATION AND CRACK CLOSURE IN AL-MG-SI ALLOYS WITH VARYING MANGANESE CONCENTRATIONS

R. Scheffel* and K. Detert*

Fatigue crack propagation of aged Al-Mg-Si alloys was studied in tests with increasing as well as decreasing cyclic stress intensities. The manganese concentration of the alloys ranged from 0 to 1 weight%. The load ratio varied between 0.1 and 0.8. A strong influence of the load ratio R was found in the range up to 0.4. due to roughness induced closure. When the crack growth data were correlated with an effective stress intensity range, the curves for the three investigated alloys fell into a common range. In a log-log plot it is composed of two parallel scatterbands each with a slope (Paris exponent) n=2 and a transition range which depends on microstructural parameters. The effective threshold value is found to be less than 2 MPa$\sqrt{m}$.

INTRODUCTION

Age hardened aluminium alloys are of great technological importance. If very high strength is required, e.g. for aircraft components, alloys of the type Al-Zn-Mg-Cu (AA 7075) are chosen. For light weight construction, in particular for ground transport systems, when good corrosion resistance is required, aluminium alloys with Mg and Si as alloying elements (Al-Mg-Si, AA 6082) are used. Since all constructions are usually subjected to alternating stresses during service, the fatigue properties of these alloys are very important.

It was found that grain size (Ruch and Gerold (1)), dispersoid content due to Mn or Cr being present (Edwards and Martin (2)) and also the stress ratio R (Scheffel and Detert (3)) are important parameters which control the fatigue properties and the fatigue crack growth rate (FCGR) at a given range of the applied cyclic stress intensity factor ΔK.

* Universität Siegen, D-5900 Siegen, FRG

This presentation is part of a study which is still going on in order to evaluate the FCG data of different Al-Mg-Si alloys in a wide interval of ΔK.

PROCEDURE

The investigated alloys were DC cast, extruded to bars and hot rolled. They were solution treated at 540°C and (under-) aged at 160°C to a hardness of 95 HB. One alloy termed Tu was commercially manufactured, the other two differ from Tu in the Mn content: Alloy MFu is manganese free, whereas MHu contains more Mn than Tu. The chemical compositions and grain sizes are compiled in Tab. 1. Average values for the mechanical properties are listed elsewhere (Detert et al. (4)).

TABLE 1 - Composition and Grain Size of the Investigated Alloys

Cast No.	MFu 41	Tu 43	MHu 45
Mg (w%)	0.91	1.02	0.89
Si (w%)	0.92	1.05	0.88
Mn (w%)	-	0.70	0.97
Fe (w%)	0.25	0.21	0.30
Grain diam. in µm	280	175	210

LT orientated CT specimens (W=100mm, B=15mm) were machined according to the ASTM specification E647-78T for tests at FCG rates above 10^{-8} m/cycle. The tests were conducted in laboratory air on a closed-loop servohydraulic testing machine under load controlled sinusodial tension testing at a frequency of 20 Hz. The specimens were cycled under stress ratios up to 0.8, such that in each cycle the maximum load depended on the stress ratio. ΔK increased continuously during the test. At every optically measured crack length a load vs. crack opening displacement (COD) record was taken to check the linearity and to correct for crack closure. This procedure is fully described in (3) for the underaged alloy Tu.

Modified Charpy specimens with a rectangular cross-section (15mm high, 10 or 5mm thick) and a 2mm notch were used in an automatic resonant fatigue testing system under pure bending to measure the FCGR below 10^{-8} m/cycle at low values of ΔK as well as to determine the threshold ΔK_{th}. The crack lengths were measured with the indirect potential drop method. During the test

the cyclic stress intensity was continuously decreased under microcomputer control using the Saxena formula (Saxena (5)):

$$\Delta K = \Delta K_{start} \exp\left[-d(a - a_{start})\right] \quad \ldots\ldots\ldots\ldots\ldots\ldots (1)$$

The system is shown in Fig. 1. Some details are reported by Berchthold (6). Either the stress ratio R or the maximum stress intensity in each cycle, K_{max}, was kept constant throughout the test. The latter procedure avoids crack closure at the threshold (Figs. 2a, b).

A strain gauge was fixed to the specimen to measure the back face strain (BFS). The BFS signal versus the applied moment was displayed on an oscilloscope again to check the linearity (e. g. the linear elastic behaviour). These curves were recorded in a handcycle after the threshold was reached. Some of the specimen were broken open for scanning electron microscopic (SEM) investigation.

RESULTS

CT-specimens. The evaluation of the FCG curves at constant stress ratio and constant load amplitude (that means at increasing ΔK) as well as the determination of the closure behaviour from load-displacement recordings is described in (3). As Figs. 3a, 4a, 5a show, the FCG curves depend on the stress ratio. It has been shown in (3) that this behaviour is caused by roughness induced closure. A micrograph of crack closure is given in Fig. 9. Crack closure also leads to the bilinear shape of the load-COD curves as discussed in (3): The intersection of the linear parts is used for the derivation of the crack opening load and the corresponding stress intensity K_{op} at each individual crack length. K_{op} depends neither on the maximum stress intensity nor on R. It is nearly constant in each test, but considerable scatter in many tests is observed. There is no significant difference in K_{op} between the three alloys. The mean value is 7.5 ± 2 MPa m.

The data of Figs. 3a, 4a, 5a are replotted in Figs. 3b, 4b, 5b as a function of

$$\Delta K_{eff} = K_{max} - K_{op} \quad \ldots\ldots\ldots\ldots\ldots\ldots\ldots\ldots (2)$$

which should be physically more significant than ΔK (see Ref. (3)). Figs. 3b, 4b, 5b support this interpretation: They show that FCG curves measured at different R coincide well in these plots whereas they did not in the original presentation. Thus the R dependence is only a result caused by crack closure.

Bending specimens. The results for alloys Tu and MFu in Figs. 6 and 7 are given as examples for FCG curves measured at gradually decreasing ΔK. Curves obtained from tests at constant R and

decreasing ΔK depend on R in the same way as curves from tests at constant R but increasing ΔK (Fig. 3a) described above. Fig. 6 shows decreasing thresholds with increasing R. The BFS vs.moment readings exibit nonlinearities, which can be used to derive K_{op} and $\Delta K_{eff,th}$ using again the bilinear construction. The results are compiled in Tab. 2. By taking $\Delta K_{eff,th}$ as a constant in the range given in Tab. 2, K_{op} could be derived for the R=0.6 curve. In this case K_{op} was not measured. The values for ΔK_{th}, $\Delta K_{eff,th}$ and K_{op} in Tab. 2 are consistent for the different stress ratios.

In contrast the curves derived under the condition K_{max} = constant are found to be independent of the value of K_{max} and since

$$K_{max} = \Delta K / (1-R) \quad \text{.....(3)}$$

these curves do not depend on R either. The fall into a common scatterband which also includes the R=0.6=constant curve down to ΔK = 2 MPa$\sqrt{m}$. Ongoing tests at constant K_{max} run into thresholds less than 1.4 MPa$\sqrt{m}$. (without indications of closure) thus confirming the $\Delta K_{eff,th}$ values in Tab. 2

TABLE 2 - Threshold Data for Alloy Tu (Bending Specimens)

R	ΔK_{th}	K_{op} (MPa$\sqrt{m}$)	$\Delta K_{eff,th}$
0.1	3.54	2.57	1.36
0.4	2.53	3.05	1.17
		3.08	1.265 (*)
0.6	1.74	3.18	1.17 (*)
		2.99	1.36 (*)

(*) $\Delta K_{eff,th}$ approximated from R=0.1 and R=0.4
K_{op} was computed using the relation

$$K_{op} = \Delta K_{th} / (1-R) - \Delta K_{eff,th} \quad \text{.....(4)}$$

All the results for the investigated alloys and testing conditions described above are compiled in Fig. 8. The data fall into a common range which is composed of two parallel scatterbands each with a slope (Paris exponent) n=2. Between them is a transition range which is different for the individual alloys.

DISCUSSION

It has been shown that crack closure due to surface roughness plays an important role in Al-Mg-Si alloys. This can be attributed to the large grain size of the present alloys. Ruch and Gerold (1, 7) found that the FCGR is lower in coarse than in fine grained Al-Mg-Si when correlated with ΔK only. They found indications for closure like aluminium oxide particles due to fretting corrosion at sliding sections of the crack surfaces only for the coarse grained material. But they did not correlate their FCG curves with ΔK_{eff}.

Since the grain size did not change the crack opening stress intensity factor too much, K_{op} was found to be fairly constant for all alloys, provided the specimen and loading geometry was not changed. K_{op} was 7.5 $MPa\sqrt{m}$ for CT- and 3 $MPa\sqrt{m}$ for the small bending specimens. This difference indicates that K_{op} cannot be regarded as a material constant, as already pointed out by McEvily (8).

The variation of the transition range in Fig. 8 can also be correlated with the grain size of our alloys: According to Yoder (9) the transition from the crystallographic to the striation mode should occur as soon as the cyclic plastic zone size exceeds the slip band length. It can increase with increasing grain size and extend the lower band in Fig. 8 to higher values of ΔK_{eff}.

The present results are in some contradiction to those given by Edwards and Martin (2) for Al-Mg-Si alloys which also contained different manganese concentrations: The FCG data at R=0.5 of their alloy containing the highest Mn concentration fits into our scheme in Fig. 8 and also shows the transition between our bands. At ΔK lower than 5 $MPa\sqrt{m}$ this curve does not match the lower band. That might happen due to closure which the authors did not correct for. They report, however, that the fracture mode changes from faceted to striated growth which agrees with our results. Their alloy with no manganese addition exhibits a very high FCGR in contrast to our results of the manganese free alloy MFu. It must be mentioned that their alloys contained a higher amount of silicon with respect to the magnesium concentration than ours did. Since the α-$Al_{12}Mn_3Si$ dispersoids cannot form in a Mn free alloy, such an alloy contains a high supersaturation of Si which might segregate at grain boundaries. Therefore they observed large portions of intergranular fatigue fracture. An increase of the FCGR due to crack propagation along grain boundaries of an aluminium alloy was also found by Nunomura et al (10).

The coincidence of all FCG curves in Fig. 8, whatever the test condition, shows that there is no real influence of stress ratio o test frequency on FCG as long as crack closure is properly taken into account. The upper band is connected with a striation mechanism of crack growth, whereas the lower one is dominated by a

crystallographic (faceted) mode, which is shown in Fig. 10 for the near threshold FCG of alloy MFu. The bands in Fig. 8 can be expressed by a modified Paris equation:

$$da/dN = C\ (\Delta K_{eff}/E)^2 \quad \ldots\ldots\ldots\ldots\ldots\ldots\ldots\ldots (5)$$

with C = 8 (0.8) for the upper (lower) band. This was already pointed out in (3) and is in good agreement with a similar result for steels given by Hahn et al. (11). That a normalization of ΔK_{eff} with the elastic modulus, $\Delta K_{eff}/E$, is meaningful can also be concluded from the scatterbands of three aluminium alloys and five steels with different microstructures measured by Lewis (12). The scatterbands between the alloys are shifted by a factor of three along the ΔK axis. This is exactly the ratio between the elastic moduli. Those tests were conducted under the condition that the minimum load during each cycle was above the closure load. The indication for an intrinsic FCG threshold around 1 MPa$\sqrt{m}$ for aluminium alloys in air is in agreement with our results and also confirms the conclusions of Liaw et al. (13). The latter authors suggest an intrinsic effective FCG threshold $\Delta K_{eff,th}$ for aluminium alloys at 1.4 ± 0.5 MPa$\sqrt{m}$. They also found that the threshold normalized with the Young's modulus can be represented as

$$\Delta K_{eff,th}/E = 1.6\ 10^{-5}\sqrt{m} \quad \ldots\ldots\ldots\ldots\ldots\ldots (6)$$

for a variety of metals and alloys in air.

SYMBOLS USED

a	= Crack Length (mm)
a_{start}	= Crack Length for Starting ΔK Reduction (mm)
C	= 8 (0.8) FCG Constant, dimensionless
d	= Saxena Decays Constant (mm^{-1})
da/dN	= FCGR, Fatigue Crack Growth Rate (nm/cycle)
E	= Young's Modulus (MPa)
ΔK	= Stress Intensity Factor Range (MPa$\sqrt{m}$)
ΔK_{eff}	= Effective Stress Intensity Factor Range (MPa$\sqrt{m}$)
$\Delta K_{eff,th}$	= Effective Threshold Stress Intensity Factor Range (MPa$\sqrt{m}$)
ΔK_{start}	= Initial Stress Intensity Factor Range (MPa$\sqrt{m}$)
ΔK_{th}	= Threshold Stress Intensity Factor Range (MPa$\sqrt{m}$)

K_{max} = Maximum Stress Intensity Factor ($MPa\sqrt{m}$)

K_{min} = Minimum Stress Intensity Factor ($MPa\sqrt{m}$)

K_{op} = Crack Opening Stress Intensity ($MPa\sqrt{m}$)

R = K_{min}/K_{max} Stress Ratio

REFERENCES

(1) Ruch, W., Gerold, V., Z. Metallkunde 76 (1985), pp.338-347

(2) Edwards, L., Martin, J.W., Metal Science 17 (1983), pp.511-518

(3) Scheffel, R., Detert, K., Proc. 5th ECF Lissabon, Portugal 1984, pp.805-810

(4) Detert, K., Scheffel, R., Stünkel, R., Proc. 7th ICSMA Montreal, Canada 1985, pp.1219-1224

(5) Saxena, A., Hudak, S.J., Donald, J.K., Schmidt, D.W., J. of Testing and Evaluation, Vol.6, No.3 (1978) pp.167-174

(6) Berchthold, R., Proc. Werkstoffprüfung 1984 Bad Nauheim, Germany (1984), pp.239-248

(7) Ruch, W., Gerold, V., Proc. 4th CF, Leoben, Austria (1982), pp.383-390

(8) McEvily, A.J., Metal Science 11 (1977), pp.274-284

(9) Yoder, G.R., Cooley, L.A., Crooker, T.W., Scripta Metallurgica 16 (1982), pp.1021-1025

(10) Nunomura, S., Higo, Y., Wakui, Y., Proc. 1st Intern. Conf. on Fatigue Thresholds, Stockholm, Sweden (1981), pp.489-500

(11) Hahn, G.T. et al., AF 336-70-C-1630, Batelle Memorial Inst., Columbus, Ohio (1971)

(12) Lewis, J.A., Proc. 2nd Intern. Conf. on Fatigue and Fatigue Thresholds, Birmingham, UK, 3-7 Sept. 1984, pp.265-274

(13) Liaw, P.K., Leax, T.R., Logsdon, W.A., Acta Metall 31 (1983), pp.1581-1587

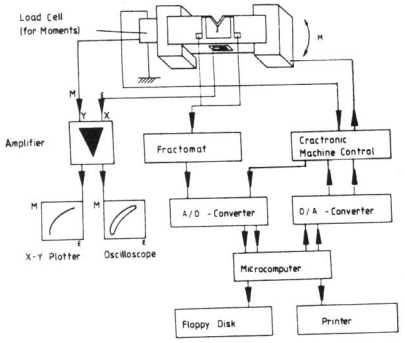

Figure 1 Threshold Testing under Computer Control

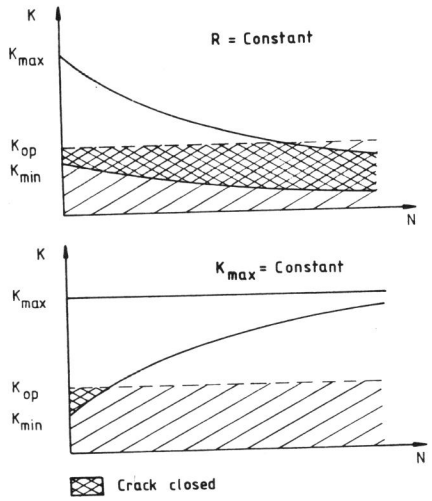

Figure 2 Variation of K
a) R=Constant b) K_{max}=Constant

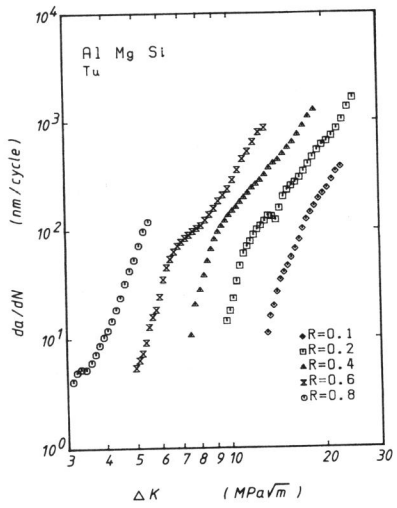

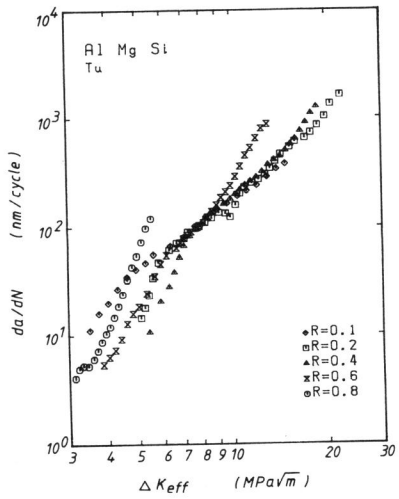

Figure 3 Fatigue Crack Growth in Alloy Tu versus
a) ΔK b) ΔK_{eff}

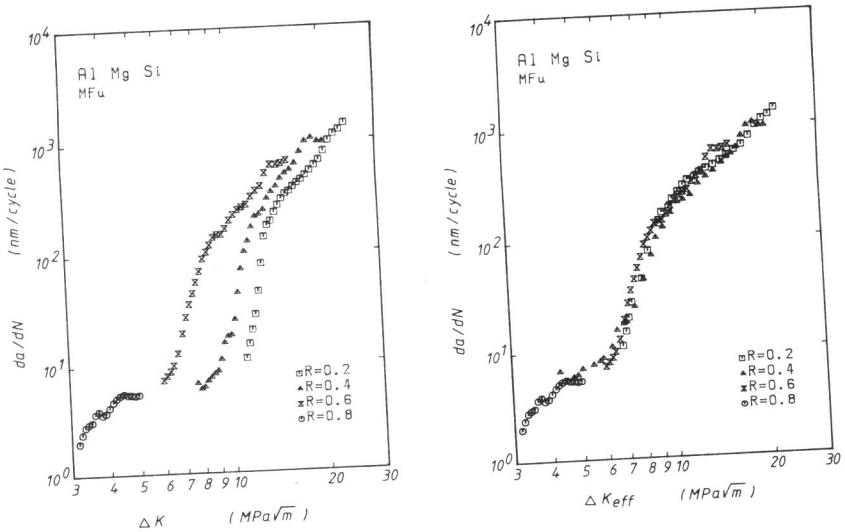

Figure 4 Fatigue Crack Growth in Alloy MFu versus
a) ΔK b) ΔK_{eff}

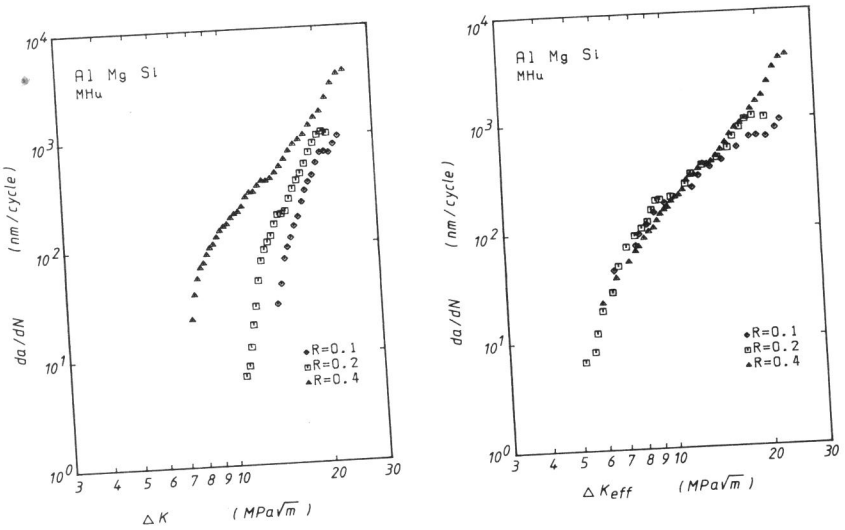

Figure 5 Fatigue Crack Growth in Alloy MHu versus
a) ΔK b) ΔK_{eff}

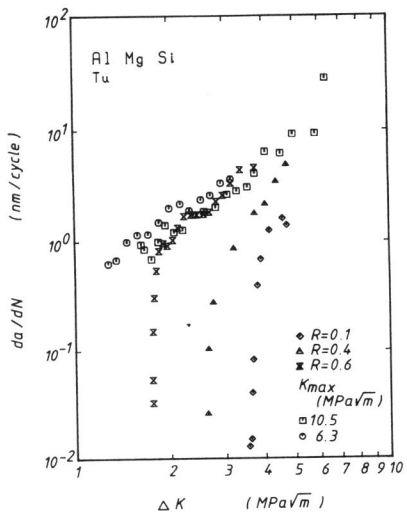

Figure 6 Near-Threshold Fatigue Crack Growth in Alloy Tu

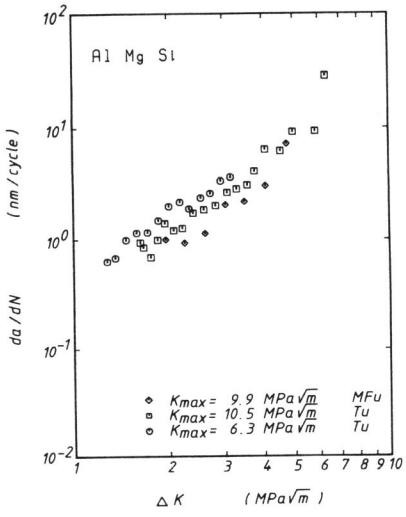

Figure 7 Near-Threshold Fatigue Growth in Alloys Tu and MFu

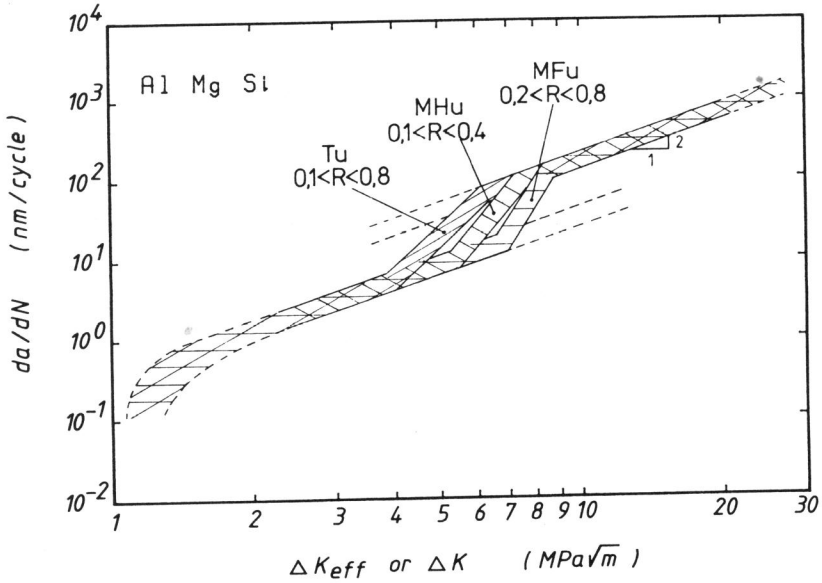

Figure 8 Comparison Figure for Fatigue Crack Growth in Al-Mg-Si Alloys

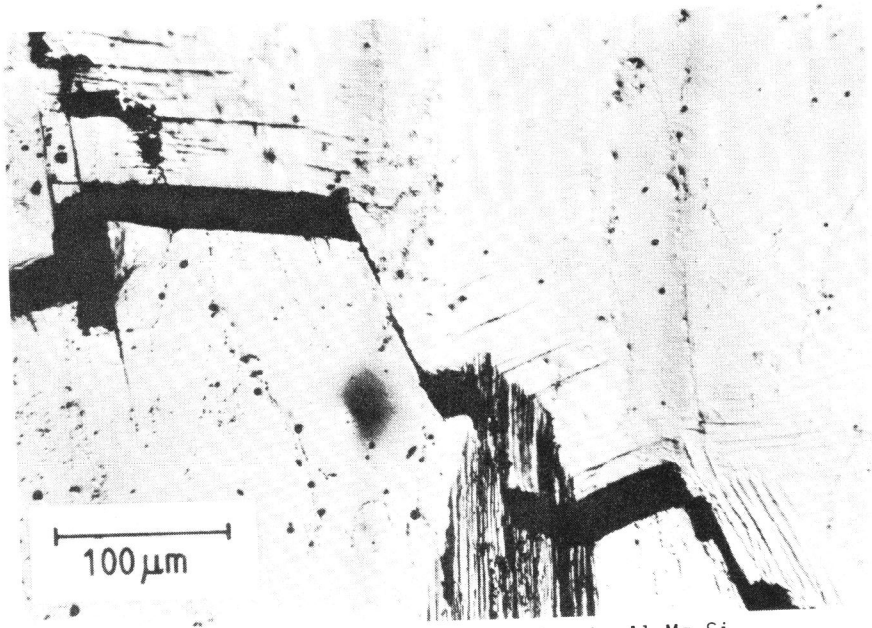

Figure 9 Typical Crack Closure Situation in Al-Mg-Si

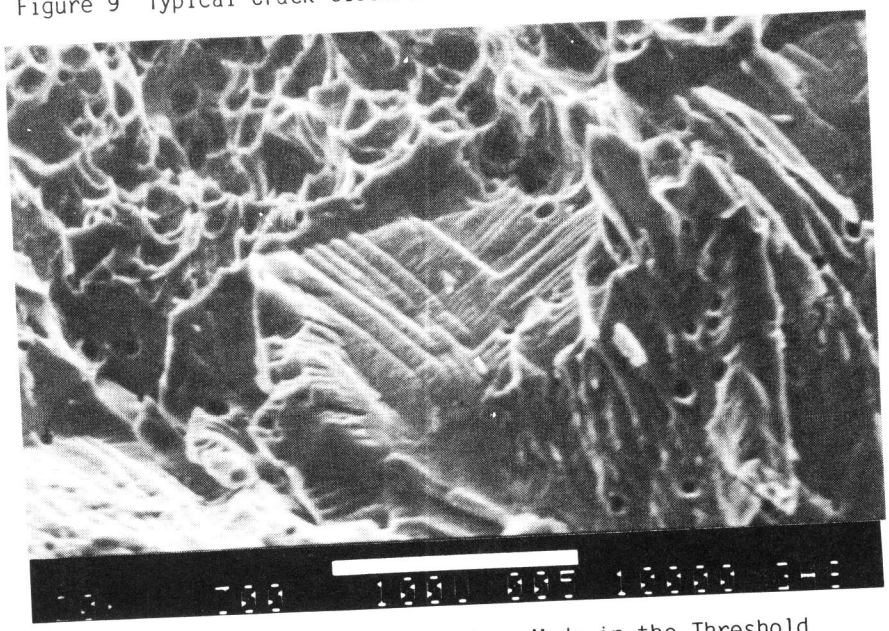

Figure 10 Crystallographic Fracture Mode in the Threshold Condition and Final Fracture in Alloy MFu